Int. J. Therm. Sci. (2000) 39, 53–62

S1290-0729(00)00195-1/FLA

A mathematical model for cooling and rapid solidification of molten metal droplets

Dirk Bergmann, Udo Fritsching *, Klaus Bauckhage

Universität Bremen, SFB 372 Sprühkompaktieren, Badgasteiner Str. 3, D-28359 Bremen, Germany

(Received 28 January 1999, accepted 3 August 1999)

Abstract — During the spray forming process, a continuous molten metal stream is atomized by impinging high speed inert gas jets. In the generated spray cone, the resulting metal droplets are rapidly cooled by the huge temperature difference to the surrounding gas phase and thereby partly solidify. After a certain flight and residence time inside the spray cone, the droplets impinge on the substrate and form the product (deposit). The material properties of this product depend on several process parameters and especially on the thermal state of the deposited droplets at impingement. Smaller droplets cool very fast and may impinge onto the product in a completely solidified state as solid metal powder particles. Larger droplets contain a higher amount of thermal energy and impact during the state of phase change or even still completely liquid. Therefore, describing the thermal history of metal droplets during flight in the spray cone is of great importance. In this contribution, a mathematical model is introduced to describe the cooling and solidification of individual metal droplets in the spray cone during the droplet–gas interaction in flight. By introducing this model into a standard two phase flow simulation model for the spray cone description, it is possible to calculate the transient droplet temperature and solid fraction contents of individual particles depending on overall process parameters and flight path. © 2000 Éditions scientifiques et médicales Elsevier SAS

rapid solidification / metal droplets / atomization / spray forming / two-phase flow simulation

Résumé — **Un modèle mathématique pour le Refroidissement et la solidification rapide de gouttelettes de métal en fusion.** Pendant le procédé de mise en forme par pulvérisation, un flux continu de métal fondu est atomisé par des jets de gaz qui le traversent. Dans le cône de pulvérisation ainsi généré, les gouttelettes de métal qui en résultent sont rapidement refroidies par l'importante différence de température avec le gaz environnant. Elles sont partiellement solidifiées après un certain temps de vol à l'intérieur du cône de pulvérisation, puis s'écrasent sur le substrat et y forment le produit (dépôt). Les propriétés du matériau obtenu dépendent de plusieurs des paramètres du procédés et spécialement de l'état thermique des gouttelettes déposées lors de l'impact. De petites gouttelettes refroidissent très vite et peuvent s'écraser sur le produit dans un état complètement solidifié ; comme le font les particules en métallurgie des poudres. De plus grosses gouttelettes contiennent une quantité plus importante d'énergie thermique et s'écrasent pendant le changement de phase liquide–solide, voire même complètement liquide. Pour ces raisons, l'historique thermique des gouttelettes de métal pendant leur vol dans le cône de pulvérisation est de grande importance. Dans cette contribution, un modèle mathématique est introduit pour décrire le refroidissement et la solidification de gouttelettes individuelles de métal dans le cône de pulvérisation pendant l'interaction gouttelette–gaz. Complant ce modèle à un modèle de simulation standard à deux écoulement de phases pour le cône de solidification, il est possible de calculer la température de transition des gouttelettes et la fraction solide de gouttelettes individuelles, chacun d'eux dépendant essentiellement des paramètres du procédé et de la trajectoire de vol. © 2000 Éditions scientifiques et médicales Elsevier SAS

solidification rapide / gouttelettes de métal / pulvérisation / simulation biphasée d'écoulement

Nomenclature

A_d	droplet surface	m^2
Bi	Biot number ($Bi = \alpha d_p/\lambda_p$)	
c_0	initial composition of the melt	weight%
c_d	specific heat capacity of the droplet	$J{\cdot}kg^{-1}{\cdot}K^{-1}$
c_l	specific heat capacity of the liquid material	$J{\cdot}kg^{-1}{\cdot}K^{-1}$
c_s	specific heat capacity of the solid material	$J{\cdot}kg^{-1}{\cdot}K^{-1}$
c_s^*	solid composition at the solid–liquid interface	weight%
$d_{50,3}$	mass median diameter	m
d_d	droplet diameter	m
f_s	fraction solid	
$f_{s,p}$	fraction solid before peritectic transformation	

* Correspondence and reprints.
ufri@iwt.uni-bremen.de

$f_{s,pe}$	fraction solid after peritectic transformation	
$f_{s,r}$	fraction solid after recalescence	
GMR	gas metal ratio ($\dot{M}_g/\dot{M}_l$)	
h	heat transfer coefficient	$W{\cdot}m^{-2}{\cdot}K^{-1}$
Δh_f	specific heat of fusion	$J{\cdot}kg^{-1}$
Δh_{fa}	atomic heat of fusion	$J{\cdot}atom^{-1}$
Δh_{fm}	molar heat of fusion	$J{\cdot}mol^{-1}$
J	nucleation rate	$s^{-1}{\cdot}m^{-3}$
k	Boltzmann constant	$J{\cdot}K^{-1}$
K	constant in equation (4)	$m^{-3}{\cdot}s^{-1}$
K_{sl}	mobility of the solid–liquid interface	$m{\cdot}s^{-1}{\cdot}K^{-1}$
k_e	equilibrium partition ratio	
m_d	droplet mass	kg
$\dot{M}_g$	gas mass flow	$kg{\cdot}s^{-1}$
$\dot{M}_l$	melt mass flow	$kg{\cdot}s^{-1}$
N_n	number of nuclei	
t	time	s
T	temperature	K
$\dot{T}$	cooling rate	$K{\cdot}s^{-1}$
T_0	initial temperature	K
T_d	droplet temperature	K
T_{fe}	melting point of pure iron	K
T_g	gas temperature	K
T_l	liquidus temperature	K
T_n	nucleation temperature	K
T_{per}	temperature of peritectic transformation	K
T_r	temperature after recalescence	K
T_s	solidus temperature	K
T_u	transformation temperature	K
ΔT	undercooling	K
ΔT_{hom}	undercooling at homogeneous nucleation	K
r	radius	m
V_m	molar volume	$m^3{\cdot}mol^{-1}$
V_a	atomic volume	$m^3{\cdot}atom^{-1}$
V_d	droplet volume	m^3
x	coordinate	m
z	coordinate	m

Greek symbols

ε	emissivity	
λ_d	thermal conductivity of the droplet	$W{\cdot}m^{-1}{\cdot}K^{-1}$
λ_g	thermal conductivity of the gas	$W{\cdot}m^{-1}{\cdot}K^{-1}$
ρ_d	droplet density	$kg{\cdot}m^{-3}$
ρ_g	gas density	$kg{\cdot}m^{-3}$
σ	Stefan–Boltzmann constant	$W{\cdot}m^{-2}{\cdot}K^{-4}$
σ_{sl}	solid–liquid surface tension	$J{\cdot}m^{-2}$

1. INTRODUCTION

The spray forming process is an industrial process for production of near net shaped metal preforms from advanced materials and with excellent material properties. This process gains and combines the classical metallurgical processes of metal casting and metal powder sintering (powder metallurgy). Rapid cooling of the droplets in the spray cone give rise to a fine grain structure and advanced material properties. By controlling the geometry and motion of the substrate, near net shaped deposits (like billets, rings and tubes, plates) may be produced. In *figure 1*, a schematic view of the spray forming process is illustrated. The material is heated in the crucible until the required super-heat temperature is reached and the melt is poured into the tundish. Crucible and tundish are located in the melting device on top of the spray chamber. The cylindrical melt stream flows in the direction of gravity into the atomization region where the molten metal stream disintegrates into droplets due to impinging gas jets. The resulting spray contains droplets with an approximate diameter range between 5 μm and 500 μm depending on operational conditions as gas pressure, gas and metal properties and atomizer geometry. For low carbon steel atomization, the mass median droplet diameter of the particle size distribution is about 60–110 μm [1].

Next to the atomization process, the molten droplets are accelerated and cooled in the spray cone. Depending on size, heat content and cooling rate, the droplets are liquid, partially liquid (changing phase, in the mushy state), or even completely solidified when they impact onto the surface of the substrate or the deposit, respectively (*figure 2*). The impacting droplet mass consolidates and forms the deposit. The shape of the deposit depends on the geometry of the spray cone and the movement of the substrate and the spray. In *figure 1* as an example, a billet is spray formed by spraying on an inclined rotating disc as substrate.

In order to improve the quality and homogeneity of the deposit in terms of microstructure and to improve the yield, it is most important to determine and control the conditions of the droplets prior to impingement. These conditions have to be derived for all individual particles to analyse the local structure and also for their drop size averaged distribution, as the temporal average values and the derivation of the local mass flux, the heat content, the fraction solid and the local size distribution of the droplets in the spray [2].

To describe the droplet–gas interaction in the spray, a mathematical model based on the Eulerian–Lagrangian approach is established to calculate the coupled two

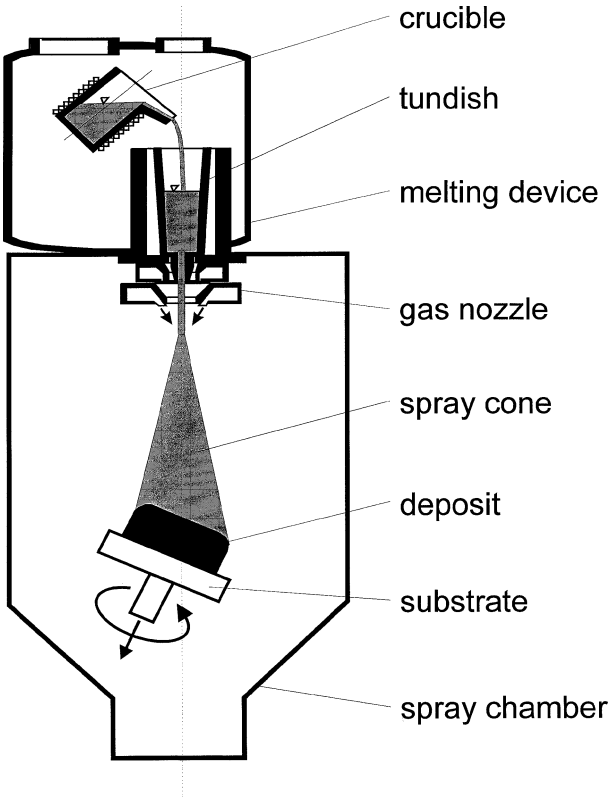

Figure 1. Schematic of a spray forming unit.

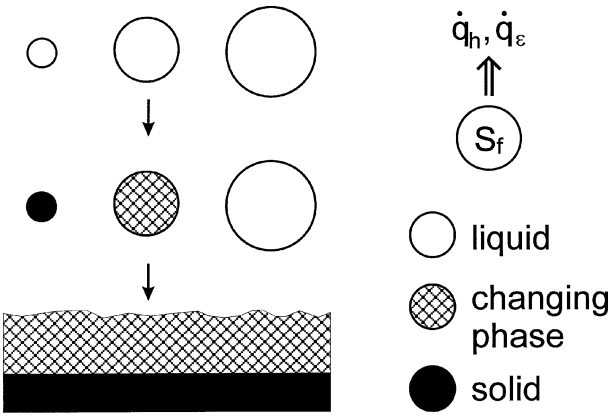

Figure 2. Droplet solidification inside the spray cone.

phase flow field in the spray chamber. In this model, the time averaged Navier–Stokes equations in combination with a standard turbulence model plus the equation for conservation of thermal energy are solved for the gas phase. Source terms for energy and momentum transfer between the gas phase and droplets are taken into account. Therefore, two way coupling for momentum and

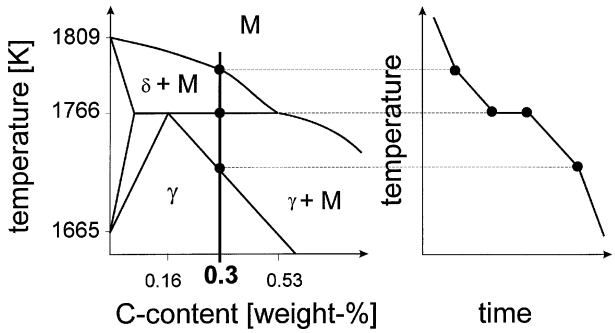

Figure 3. Iron-carbon phase diagram and derived cooling curve.

thermal energy is achieved. The total number of droplets in the spray hereby is represented by tracking a series of parcel trajectories [3].

In comparison to similar models described in literature, this model is not related to a constant preset gas velocity and temperature field. Their distributions are calculated as part of the multidimensional computation, depending on process parameters and geometry and based on gas–droplet interaction (two way coupling). Therefore, it is possible to predict the thermal condition of the droplets according to operation conditions and local position of the droplets inside the spray cone.

Different materials and alloys are used for spray forming in an industrial context like steel, copper and aluminium. One of the key submodels for numerical description of the spray forming process is a matched solidification model, depending on the base material and alloy composition.

2. SOLIDIFICATION MODEL

The solidification model described in this contribution is developed for low carbon steel C30 (0.3 weight% C) but is easily adapted to other material compositions.

Figure 3 shows part of the iron-carbon phase diagram, where the area for C30 is highlighted. For low cooling rates in equilibrium, the shown temperature versus time curve can be derived directly from this phase diagram. In fact in spray processes the cooling rate of droplets especially immediately after atomization might be very high. Therefore, the possibility of undercooling prior to nucleation and the outset of solidification has to be considered. In *figure 4* a typical qualitative temperature distribution for a single droplet in a metal droplet spray is shown. Starting with the initial melt temperature (superheated) T_m, the droplet cools down to liq-

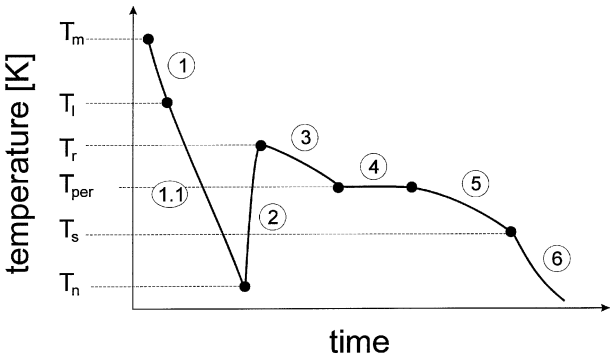

Figure 4. Qualitative cooling curve of droplet in spray cone.

uidus temperature T_l. Depending on the actual cooling rate, the droplet may undercool until it reaches the nucleation temperature T_n before solidification starts. Due to the rapid release of latent heat of fusion during recalescence, the droplet temperature increases until it reaches a local maximum in the cooling curve at T_r. During the following segregated solidification, droplet temperature decreases continuously. At temperature T_per, the peritectic transformation takes place at constant droplet temperature. After termination of the peritectic transformation, again segregated solidification occurs until the droplet is completely solidified at T_s. From here on, droplet cooling is in the solid state of the fully solidified particle. In the following, the different states of droplet cooling and solidification will be separately analysed.

2.1. Cooling in the liquid state

For a spherical droplet, the change of internal heat contents according to convection and radiation heat transfer can be expressed by:

$$c_{\mathrm{d,l}}\frac{\mathrm{d}T_\mathrm{d}}{\mathrm{d}t} = -\frac{6h}{\rho_\mathrm{d} d_\mathrm{d}}(T_\mathrm{d} - T_\mathrm{g}) - \frac{6\varepsilon\sigma}{\rho_\mathrm{d} d_\mathrm{d}}\left(T_\mathrm{d}^4 - T_\mathrm{w}^4\right) \qquad (1)$$

where T_d is the droplet temperature, T_g the gas temperature and T_w the temperature of the surrounding walls. The specific heat capacity of the liquid droplet material is $c_{\mathrm{d,l}}$, h is the heat transfer coefficient, ε and σ are the emissivity and Stefan–Boltzmann constant, ρ_d and d_d are the droplet's density and diameter, respectively. An internal temperature gradient inside the droplet is neglectable, because of the high thermal conductivity of metals and therefore very low Biot numbers ($Bi \ll 1$) for all metal droplets which are taken into consideration.

2.1.1. Undercooling

When the droplet temperature reaches the liquidus of the material, the solidification process does not immediately start. Depending on cooling rate and droplet size, the temperature T_n where nucleation occurs can be much lower than the liquidus temperature T_l. The nucleation temperature for continuous cooling is defined as the temperature, where the number of nuclei N_n in the droplet volume V_d is identical to one:

$$N_\mathrm{n} = V_\mathrm{d}\int_{T_\mathrm{l}}^{T_\mathrm{n}} \frac{J(T)}{\dot{T}}\,\mathrm{d}T = 1 \qquad (2)$$

Here, $J(T)$ is the nucleation rate and $\dot{T}$ the cooling rate [4, 5]. Hirth [6] has shown that equation (2) may be simplified to:

$$\frac{0.01 J(T_\mathrm{n}) V_\mathrm{d} \Delta T_\mathrm{hom}}{\dot{T}} \approx 1 \qquad (3)$$

where ΔT_hom is the undercooling temperature difference for homogeneous nucleation. The nucleation rate may be expressed as [6, 7]:

$$J(T_\mathrm{n}) = K \exp\left(-\frac{16\pi\sigma_\mathrm{sl}^2 V_\mathrm{m}^2 T_\mathrm{l}^2}{3kT_\mathrm{n}\Delta h_\mathrm{fm}^2 \Delta T_\mathrm{hom}^2}\right) \qquad (4)$$

with σ_sl as solid–liquid interfacial energy and Δh_fm as molar latent heat of fusion. From measurements the preexponential factor K is derived to 10^{41} $\mathrm{m^{-3}{\cdot}s^{-2}}$ [6, 7]. In the work of Turnbull [8] and Woodruff [9], a correlation between the solid–liquid interfacial energy, the latent heat of fusion per atom Δh_fa and the atomic volume V_a is given by

$$\sigma_\mathrm{sl} = 0.45\Delta h_{\mathrm{f,a}} V_\mathrm{a}^{-2/3} \qquad (5)$$

It is well known that in technical processes, heterogeneous nucleation rather than homogeneous nucleation mechanisms limit the degree of undercooling. Only in very small droplets homogeneous nucleation plays an important role during solidification. Based on experimental results for different alloys, Mathur et al. [2] derived the following exponential correlation between the actual undercooling ΔT and the amount of undercooling necessary for homogeneous nucleation, which can be formulated as [10]

$$\Delta T = \Delta T_\mathrm{hom} \exp\left(-2.2{\cdot}10^{12} V_\mathrm{d}\right) \qquad (6)$$

Once the actual undercooling is calculated based on the previous set of equations, the actual nucleation

temperature for a droplet is determined by

$$T_\mathrm{n} = T_\mathrm{l} - \Delta T \tag{7}$$

In this model the maximum value of undercooling is limited based on the results of Turnbull [8], e.g., the maximum undercooling for iron based alloys is 295 K. Also a minimum undercooling of 3 K is assumed.

2.2. Recalescence

After nucleation has started, the solidification process of a droplet obtains an internal heat source due to release of latent heat of fusion. The conservation equation for the droplet thermal energy has to be extended with a corresponding term to

$$c_\mathrm{d}\frac{\mathrm{d}T_\mathrm{d}}{\mathrm{d}t} = \Delta h_\mathrm{f}\frac{\mathrm{d}f_\mathrm{s}}{\mathrm{d}t} - \frac{6h}{\rho_\mathrm{d} d_\mathrm{d}}(T_\mathrm{d} - T_\mathrm{g}) - \frac{6\varepsilon\sigma}{\rho_\mathrm{d} d_\mathrm{d}}\left(T_\mathrm{d}^4 - T_\mathrm{w}^4\right) \tag{8}$$

with f_s as fraction solid ($f_\mathrm{s} = 0$: droplet is completely liquid; $f_\mathrm{s} = 1$: droplet is completely solid) and the specific heat capacity of the droplet c_d as the average of the solid and liquid content:

$$c_\mathrm{d} = f_\mathrm{s} c_\mathrm{ds} + (1 - f_\mathrm{s}) c_\mathrm{dl} \tag{9}$$

The solidification kinetics in equation (8) may be transformed into the following expression:

$$\frac{\mathrm{d}f_\mathrm{s}}{\mathrm{d}t} = \frac{\mathrm{d}f_\mathrm{s}}{\mathrm{d}x}\,\frac{\mathrm{d}x}{\mathrm{d}t} \tag{10}$$

Assuming that a single nucleation event at the surface of the droplet starts the solidification process and the curvature of the solid–liquid interface during recalescence is equal to the droplet surface curvature, the change of the solid fraction along the growth axis is given by [11]

$$\begin{aligned}\frac{\mathrm{d}f_\mathrm{s}}{\mathrm{d}x} &= \left[\frac{3}{2}\left(\frac{x}{d_\mathrm{p}}\right)^2 - \frac{1}{2}\left(\frac{x}{d_\mathrm{p}}\right)^3\right]' \\ &= \frac{1}{d_\mathrm{p}}\left(3\left(\frac{x}{d_\mathrm{p}}\right) - \frac{3}{2}\left(\frac{x}{d_\mathrm{p}}\right)^2\right)\end{aligned} \tag{11}$$

The velocity of the solid–liquid interface movement is approximated as a linear crystal growth rate function of undercooling:

$$\frac{\mathrm{d}x}{\mathrm{d}t} = K_\mathrm{sl}\left[T(f_\mathrm{s}) - T_\mathrm{p}\right] = K_\mathrm{sl}\Delta T \tag{12}$$

In this equation, K_sl is the solid–liquid interfacial mobility, having a magnitude of 0.01 $\mathrm{m{\cdot}s^{-1}{\cdot}K^{-1}}$ [4, 11, 12]. The phase of recalescence ends, when the production rate of internal heat equals the heat transfer from the droplet surface. Here, the cooling curve of a droplet reaches a local maximum (*figure 4*) and the droplet temperature equals T_r:

$$\Delta h_\mathrm{f}\frac{\mathrm{d}f_\mathrm{s}}{\mathrm{d}t} = \frac{6h}{\rho_\mathrm{d} d_\mathrm{d}}(T_\mathrm{r} - T_\mathrm{g}) + \frac{6\varepsilon\sigma}{\rho_\mathrm{d} d_\mathrm{d}}\left(T_\mathrm{r}^4 - T_\mathrm{w}^4\right) \tag{13}$$

2.3. Segregated solidification 1

The further solidification process after recalescence takes place again with a decrease in droplet temperature. The heat conservation equation in this stage is described by

$$\begin{aligned}&\frac{\mathrm{d}T_\mathrm{d}}{\mathrm{d}t}\left(c_\mathrm{d} + \Delta h_\mathrm{f}\frac{\mathrm{d}f_\mathrm{s}}{\mathrm{d}T_\mathrm{d}}\right) \\ &\quad = -\frac{6h}{\rho_\mathrm{d} d_\mathrm{d}}(T_\mathrm{d} - T_\mathrm{g}) - \frac{6\varepsilon\sigma}{\rho_\mathrm{d} d_\mathrm{d}}\left(T_\mathrm{d}^4 - T_\mathrm{w}^4\right)\end{aligned} \tag{14}$$

The increase of solid fraction with droplet temperature is assumed according to Scheil's equation [13]:

$$c_\mathrm{s}^* = k_\mathrm{e} c_0 (1 - f_\mathrm{s})^{k_\mathrm{e}-1} \quad \text{with } c_\mathrm{s}^* = k_\mathrm{e} c_\mathrm{l} \tag{15}$$

where c_s^* is the composition of solid at the solid–liquid interface, c_0 is the initial composition of the material and k_e is the equilibrium partition ratio. This relation can be transformed into

$$\begin{aligned}f_\mathrm{s} &= 1 - (1 - f_\mathrm{s,r})\left(\frac{c_\mathrm{l}}{c_0}\right)^{1/(k_\mathrm{e}-1)} \\ &= 1 - (1 - f_\mathrm{s,r})\left(\frac{T_\mathrm{fe} - T_\mathrm{d}}{T_\mathrm{fe} - T_\mathrm{l}}\right)^{1/(k_\mathrm{e}-1)}\end{aligned} \tag{16}$$

and

$$\frac{\mathrm{d}f_\mathrm{s}}{\mathrm{d}T_\mathrm{d}} = \frac{1 - f_\mathrm{s,r}}{(k_\mathrm{e} - 1)(T_\mathrm{fe} - T_\mathrm{d,r})}\left(\frac{T_\mathrm{fe} - T_\mathrm{d}}{T_\mathrm{fe} - T_\mathrm{d,r}}\right)^{(2+k_\mathrm{e})/(k_\mathrm{e}-1)} \tag{17}$$

with T_fe as liquidus temperature of pure iron as base material and $T_\mathrm{d,r}$ and $f_\mathrm{s,r}$ as the solid fraction and temperature of the droplet after recalescence, respectively.

2.4. Peritectic transformation

When the droplet temperature reaches the peritectic temperature, it remains at a constant value until this phase

transformation is terminated. The change in solid fraction during peritectic solidification is described by:

$$\Delta h_f \frac{df_s}{dt} = -\frac{6h}{\rho_d d_d}(T_d - T_g) - \frac{6\varepsilon\sigma}{\rho_d d_d}\left(T_d^4 - T_w^4\right) \quad (18)$$

Peritectic solidification ends, when the composition of the remaining liquid reaches the appropriate concentration. Based on phase diagram, it is possible to calculate the solid fraction $f_{s,pe}$ according to this concentration:

$$f_{s,pe} = \frac{0.53 - c_0}{0.53 - 0.16} = 0.622 \quad (\text{for } c_0 = 0.3 \text{ weight\%}) \quad (19)$$

2.5. Segregated solidification 2

Further segregated solidification takes place in the droplet after peritectic transformation and can be described by the assumptions shown in Section 2.3.

2.6. Cooling in the solid state

After the droplet is completely solidified, it further cools down in the solid state. This process can be evaluated from the following equation:

$$c_{ds}\frac{dT_d}{dt} = -\frac{6h}{\rho_d d_d}(T_d - T_g) - \frac{6\varepsilon\sigma}{\rho_d d_d}\left(T_d^4 - T_w^4\right) \quad (20)$$

with c_s as the specific heat capacity of the solid material.

This solidification model is interpreted as a submodel into the numerical simulation model of the spray cone behaviour, taking into account the two way coupling of momentum and heat.

3. RESULTS

Results are calculated and will be shown based on two different sets of process parameters representing two different atomizer gas pressures. The atomizer gas pressure is the most important online control parameter of the spray forming process. In both sets materials properties for C30 steel are used, the melt's superheat prior to atomization is 100 K and the melt mass flow rate is 0.192 kg·s^{-1}. The mass flow ratio for gas and melt (GMR: gas–metal ratio) is varied from 1.1 to 1.5 by increasing the gas mass flow rate. At these operation conditions the mass median droplet diameter of

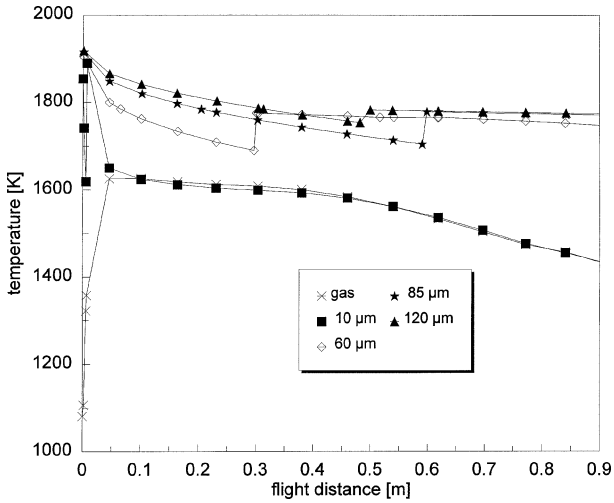

Figure 5. Cooling curves for different droplet sizes, flight path in the core region of the spray cone at a GMR of 1.5.

the particle size distribution only marginally varies at about 85 µm [1]. Therefore, the following results of this investigation are shown based on a constant particle size for a specific discussion of the effect of the GMR only on the droplet cooling process inside the spray cone.

After atomization, the melt droplets are accelerated and cooled down by the gas stream. Starting with the initial melt temperature, the droplets temperature history depends on their size and flight path in the spray cone. In *figure 5*, cooling curves for four different droplet sizes representing the droplet size distribution in comparison to the calculated gas temperature along flight distance in the core (centre line) of the spray are shown. Due to the locally high concentration of droplets in the core, here the gas temperature increases very rapidly and reaches a sudden maximum in a distance 5.5 cm below the atomization area. Subsequently, the gas temperature decreases, due to mixing with entrained colder gas from surrounding regions.

The smallest calculated (10 µm) droplet fraction cools down fastest and establishes the highest degree of undercooling. In a specific distance from the atomization area, these droplets yield the same temperature as the gas and follow its trend. The largest droplets cool down slower, according to their higher mass. Their temperature at the end of the computed flight distance is close to the melting point (1785 K).

In contrast to droplets moving in the core region of the spray, the temperature of droplets moving within the edge region of the spray cone decreases much faster (*figure 6*). Here, these droplets are in direct contact with the colder ambient gas. Therefore, the temperatures of gas and

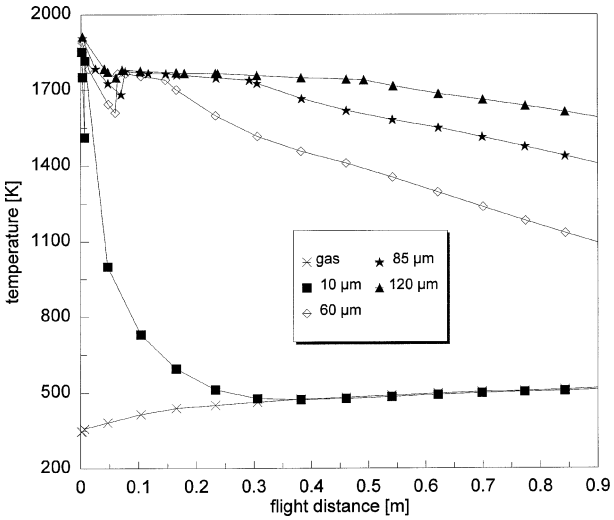

Figure 6. Cooling curves for different droplet sizes, flight path in the edge region of the spray cone at a GMR of 1.5.

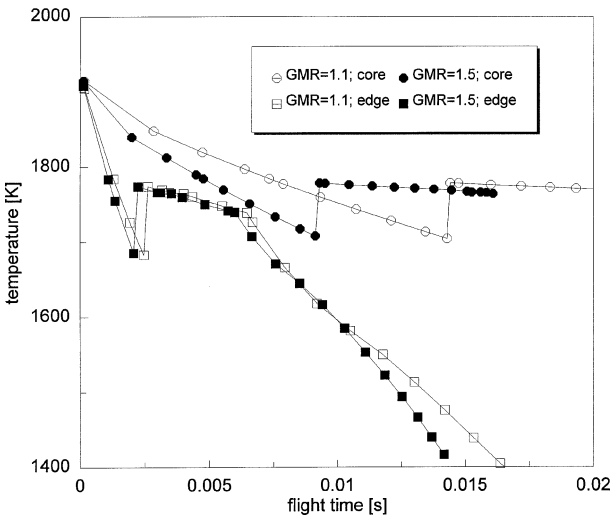

Figure 7. Temperature versus flight time of 85 µm droplets flying in the core region and in the edge region of the spray cone at a GMR of 1.1 and 1.5.

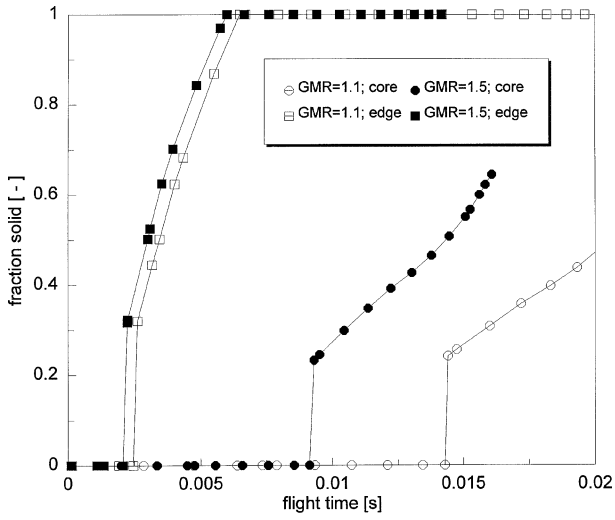

Figure 8. Fraction solid versus flight time of 85 µm droplets flying in the core region and in the edge region of the spray cone at a GMR of 1.1 and 1.5.

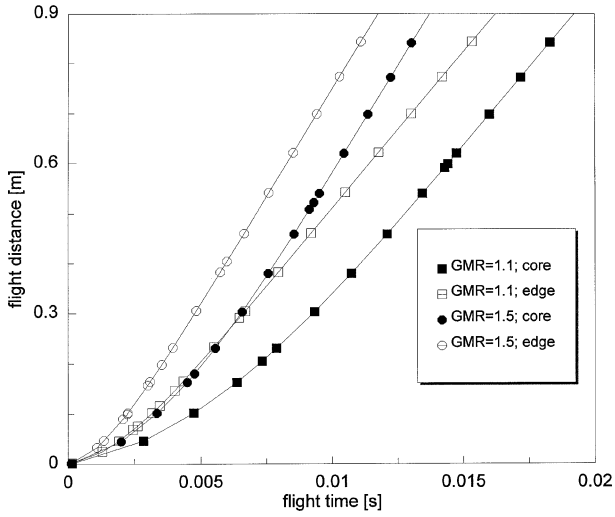

Figure 9. Flight distance versus flight time of 85 µm droplets flying in the core region and in the edge region of the spray cone at a GMR of 1.1 and 1.5.

droplets reach a much lower level. After a flight distance of about 0.58 m, the temperatures of all displayed droplet sizes are below the solidification temperature.

An increase in GMR leads to higher cooling rates of the droplets. In *figure 7* and *figure 8* the temperatures and the solid fraction of a 85 µm droplet versus flight time for different GMR and flight paths are shown. The droplets in the edge region of the spray cone at a higher GMR cool fastest followed by the droplets with the same flight path at a lower GMR. The 85 µm droplets flying in the spray core region at the lower GMR cool down slowest. The sudden increase in the solid fraction curves is a result of the fast solidification process during recalescence after undercooling.

Besides droplet cooling, a change in GMR also effects the droplet velocity. In *figure 9* the calculated flight distance of droplets is shown versus the flight time and in *figure 10* the droplet velocity is shown versus flight distance. The fastest droplets can be found within the edge region of the spray cone at the higher GMR value. These droplets receive the lowest residence time inside

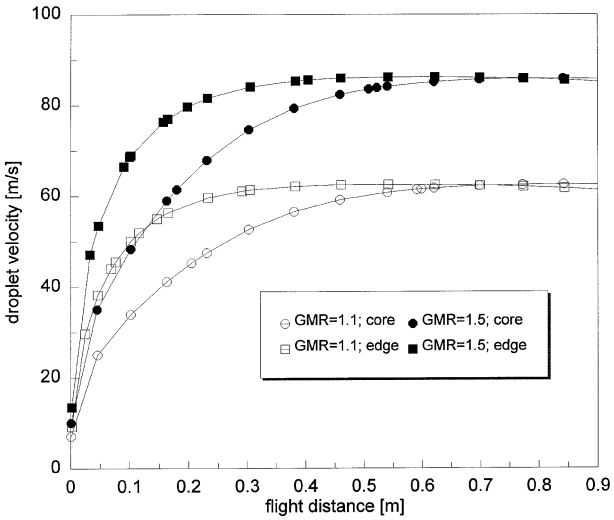

Figure 10. Velocity versus flight distance of 85 μm droplets flying in the core region and in the edge region of the spray cone at a GMR of 1.1 and 1.5.

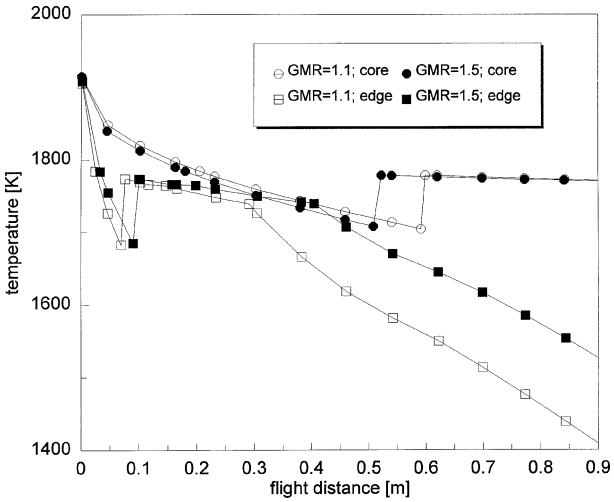

Figure 11. Temperature versus flight distance of 85 μm droplets flying in the core region and in the edge region of the spray cone at a GMR of 1.1 and 1.5.

the spray during flight from the atomization to the impingement area.

Apart from temperature gradients and flow conditions, the overall heat loss of a droplet depends on its residence time inside the spray cone. This effect clearly illustrates why the 85 μm droplets moving at the edge region of the spray at the higher GMR are still hotter and less solidified than the droplets travelling in the same region but at a lower GMR (*figure 11* and *figure 12*).

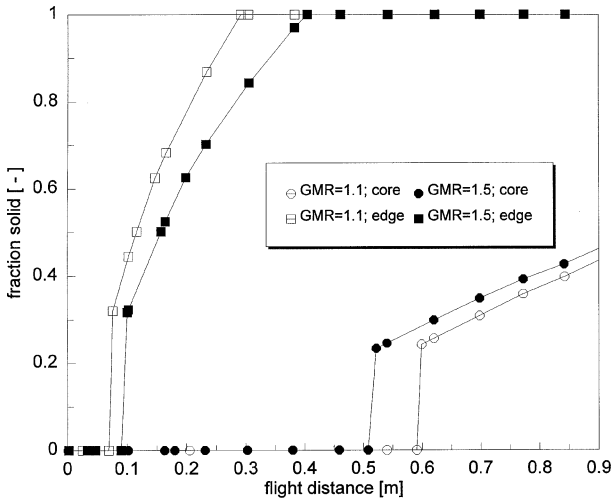

Figure 12. Fraction solid versus flight distance of 85 μm droplets flying in the core region and in the edge region of the spray cone at a GMR of 1.1 and 1.5.

The results about droplet cooling inside the spray cone can be used to explain defects of the deposit material which may appear during the spray forming process. If the impacting droplet mass is too hot, an undesired coarsening of the grain size distribution may occur, especially in the centre of the deposit. In contrast to that, too cold droplets are responsible for the formation of porosity. This happens particularly in the edge zones of the deposit.

The above considerations exemplifies the importance of a detailed analysis of the thermal conditions of droplets hitting the surface of the substrate/deposit during the spray forming process. A difference has to be made between position of impact, respectively flight path, flight time, droplet size and alloy composition. The described numerical model has the potential to support these investigations. In combination with spray forming experiments, this model is used to find the best parameter set to produce homogeneous deposits of good quality.

4. MODEL VERIFICATION

The verification of the model is done indirectly. By using two different averaging methods [14], the mean temperature of the overall droplet mass (sum of all droplets at one position) is calculated and compared with pyrometric temperature measurements of the deposit surface during spray forming. The averaging methods differ in the basic assumptions. For the first method it is assumed that the droplet mass is in the state of

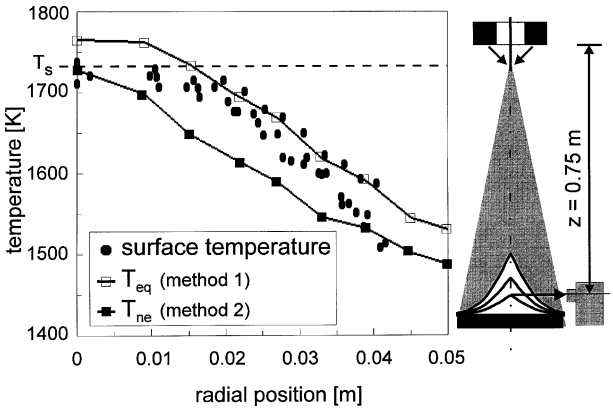

Figure 13. Mean droplet temperature and measured surface temperature of the deposit versus radial position.

thermal equilibrium. Therefore, the mean temperature is calculated from the mass mean enthalpy according to the phase diagram. In the second method, the mean droplet temperature is determined from the heat content (droplet temperature times specific heat) and the mean solid fraction is separately calculated from the remaining heat of fusion of the droplets.

The measurements of the deposit surface temperature are done using a stationary pyrometer facing toward the top of a Gaussian shaped deposit. During the deposit growth, the measurement point moves to larger radial positions [1]. The comparison between calculated and measured temperatures and a sketch of the experimental set-up are shown in *figure 13*.

Both the calculated and the measured temperatures decrease with lager radial distance from the spray cone centre. The calculated temperatures shows a good agreement with the measurements. All temperatures are below the solidus temperature, except those close to the centreline. The measured values are between the calculated mean temperatures determined with method 1 and method 2, respectively, as the two averaging methods represent two extreme temperature values as upper and lower boundary.

5. CONCLUSION

Motivation for the described investigations is to predict the thermal conditions of metal particles impacting onto the pre-product during the spray forming process. The heat content and the solid fraction of these droplets has a significant influence on the overall cooling process of the product and therefore on its quality in terms of microstructure.

In order to predict the thermal conditions of metal particles during the spray forming process, a numerical solidification model is described and a multiphase flow model is established to calculate droplet temperatures and solid fractions depending on main process parameters like gas–metal ratio (GMR) and the droplet's flight path inside the spray cone. The solidification model describes the different stages during phase change of a molten metal droplet, starting with an initial superheat temperature down to the temperature of the completely solidified droplet. The special properties of the materials are taken into account. Sample calculations using this model obtain a strict dependency of the droplet cooling behaviour on flight path of the droplets inside the spray cone and on gas to metal mass flow ratio (GMR).

Acknowledgements

The authors would like to acknowledge the financial support by the Deutsche Forschungsgemeinschaft (DFG) in the SFB 372 Spray Forming.

REFERENCES

[1] Kramer C., Die Kompaktierungsrate beim Sprühkompaktieren von Gauß-förmigen Deposits, Ph.D. Thesis, University of Bremen, 1997.

[2] Mathur P., Apelian D., Lawley A., Analysis of the spray deposition process, Acta Metall. 2 (1989) 429–443.

[3] Bergmann D., Fritsching U., Crowe C.T., Multiphase flow in the spray forming process, in: 2nd International Conference on Multiphase Flow, Kyoto, Japan, 1995.

[4] Lavernia E.J., Wu Y., Spray Atomization and Deposiston, John Wiley & Sons, Ltd., Chichester, 1996.

[5] Pryds N.H., Hattel J.H., Numerical modelling of rapid solidification, Modelling Simul. Mater. Sci. Eng. 5 (1997) 451–472.

[6] Hirth J.P., Nucleation, undercooling and homogeneous structures in rapidly solidified powders, Metallurgical Transactions A 3 (1978) 401–404.

[7] Libera M., Olsen G.B., Van der Sande J.B., Heterogeneous nucleation of solidification in atomized liquid metal droplets, Materials Science and Engineering A132 (1991) 107–118.

[8] Turnbull D., Formation of crystal nuclei in liquid metals, J. Appl. Phys. 21 (1950) 1022–1028.

[9] Woodruff D.P., The Solid–Liquid Interface, Cambridge University Press, Cambridge, 1973.

[10] Li B., Liang X., Earthman J.C., Lavernia E.J., Two dimensional modelling of momentum and thermal behaviour during spray atomization of γ-TiAl, Acta Mater. 6 (1996) 2409–2420.

[11] Lee E.S., Ahn S., Solidification progress and heat transfer analysis of gas-atomized alloy droplets during spray forming, Acta Metall. Mater. 9 (1994) 3231–3243.

[12] Wang G.X., Matthys E.F., Numerical modelling of phase change and heat transfer during rapid solidification processes: Use of control volume integrals with element subdivision, Int. J. Heat Mass Transfer 1 (1992) 141–153.

[13] Brody H.D., Flemings C., Solute redistribution in dendritic solidification, Transactions of the Metallurgical Society of AIME 5 (1966) 615–623.

[14] Bergmann D., Fritsching U., Bauckhage, K., Averaging thermal conditions in molten metal sprays, in: Proceedings of the TMS-Minerals, Metals & Materials Soc., TMS Annual Meeting, San Diego, USA, 1999, pp. 129–138.